CONFIRMING CENTRIFUGAL COMPRESSOR AERODYNAMIC PERFORMANCE USING LIMITED TEST DATA COMBINED WITH COMPUTATIONAL FLUID DYNAMIC TECHNIQUES

by

Shreekant Shah

Senior Design Engineer

and

John Bartos

Director of Custom Centrifugal Compressor Operations

A-C Compressor Corporation

Appleton, Wisconsin

Shreekant Shah has been Senior Design Engineer at A-C Compressor Corporation in Appleton, Wisconsin, for the past two and one-half years. His primary responsibilities include aerodynamic design of centrifugal compressors and development. Previously, he was a Technical Partner for 10 years at Hi-Speed Turbodrives, a company manufacturing centrifugal fans and blowers, and was a Design Engineer for three years at Roots-Dresser, where he was involved in the design of centrifugal compressors.

Mr. Shah received a B.S.M.E. degree from Sardar Patel University, Gujarat, India (1977) and an M.S.M.E. degree from the Indian Institute of Technology, Bombay, India (1979).

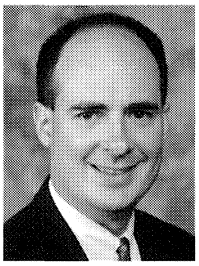

John C. Bartos is Director of Custom Centrifugal Compressor Operations with A-C Compressor Corporation, in Appleton, Wisconsin. He is responsible for the application, design, development, and management of their multistage and high pressure single-stage compressor lines. He has been with A-C for more than three years and had previously served as the Director of Engineering for their engineered products business. Mr. Bartos' experience includes areas of compressor performance calculations, aerodynamic design, machinery component design, structural analysis, and rotordynamics. Prior to joining A-CCC, he served as Product Manager, Centrifugal Compressors with Conmec, Inc. and was a Design Engineer with Ingersoll-Rand's Engineered Pump and Turbomachinery Divisions.

Mr. Bartos received his Bachelor of Engineering degree from Stevens Institute of Technology.

ABSTRACT

Facing increased market demands for improved aerodynamic efficiency, centrifugal compressor manufacturers must be able to predict and quote the best performance available from the machinery they produce. Confidence in these predictions allows manufacturers to remain competitive while avoiding the possibility of penalties for performance not achieved and, what is most important, retain customer confidence for machinery produced. Results from hardware and model testing are used to calibrate proprietary aerodynamic selection and sizing software. The challenge presented herein involves the measurement and prediction of impeller aerodynamic performance for a single-stage centrifugal compressor for which accurate test data is very difficult to obtain. The impeller under consideration was modelled using a commercially available computational fluid dynamics (CFD) analysis code developed by a Canadian company. The measured impeller's total and static discharge pressures were compared to the CFD code's predictions and found to be in excellent agreement. However, temperature rise data across the stage proved difficult to accurately measure. Without the benefit of reliable data to calculate aerodynamic efficiency, the CFD code was used to predict the impeller's efficiency. The results of the code proved to be very close to the values for efficiency originally predicted in the design of the stage.

INTRODUCTION

This investigation involves a high inlet pressure, high volumetric flow, low head impeller designed for application in a single-stage centrifugal compressor. As a result of the impeller's low head design, a low temperature rise across the stage was predicted. This low temperature rise across the stage rendered the test measurements overly susceptible to errors. Heat transfer into the static aerodynamic elements through the casing boundaries, due to elevated bearing oil temperatures along with heat transfer through impeller and shaft, offers possible additional negative influence on the reliability of the test measurements. This study was done using TASCflow [1], a computerized analysis code developed by Advanced Scientific Computing Ltd.

With the flexibility of selecting alternate gases in order to achieve higher pressure ratios and higher temperature rise across a single-stage, it may have been feasible to obtain accurate aerodynamic performance measurements for the impeller under consideration. A closed loop test per ASME PTC 10 [2] guidelines would have been desirable for the machine in question. Unfortunately, schedule and cost constraints did not allow for such testing. The high volume flows associated with this family of compressors require prohibitively large piping and cooler configurations. The practical alternative is to use open air testing for mechanical and aerodynamic performance evaluation.

The investigation involves production hardware manufactured in fulfillment of a contract. Actual mechanical and aerodynamic performance testing was conducted with the compressor suction and discharge open to atmosphere. Along with standard test hardware, the compressor was modified to accept additional probes. Revised measurements consisted of redundant probes for temperature and pressure located at the impeller inlet and discharge. In an effort to minimize contribution from outside sources, measurements for total and static pressure and total

temperature were taken as close to the impeller inlet and discharge as practical.

COMPRESSOR DESIGN

The unit under investigation is an overhung single-stage centrifugal compressor. The compressor frame was designed to operate under moderately high suction pressures. The casing is a fabricated radially split barrel construction. It is designed to operate at a fixed speed with additional aerodynamic control afforded by means of pneumatically adjustable inlet guide vanes (IGV). Flow enters the compressor axially through the inlet and across the guide vanes. The guide vanes are located in a "tucked in" configuration that places them as close as possible to the impeller inlet for maximum effect. The impeller is a high flow coefficient, low tip speed, low head design. It is constructed without a cover as per the customer's requirements. The impeller discharges into an internal scroll insert that forms the diffuser passage and the discharge gas passage. A cross sectional view of the compressor is presented in Figure 1.

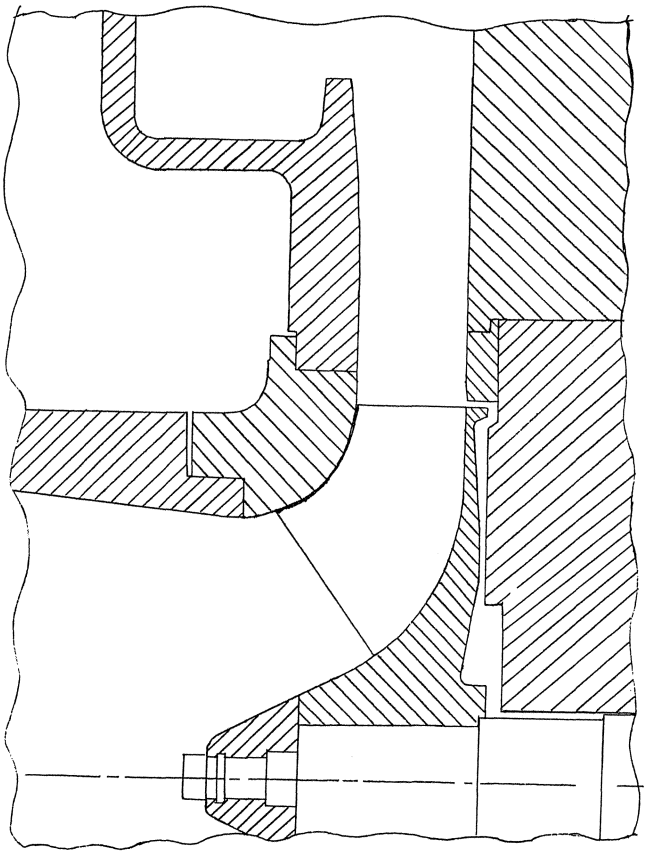

Figure 1. Cross Sectional View of the Compressor.

The nondimensional parameters for the stage are listed below.

- Specific speed: 1.55
- Inlet flow coefficient: 0.165
- Head coefficient: 0.3569
- Inlet Mach number: 0.326
- Total pressure ratio: 1.0673
- Scroll matching: 1.045

The nondimensional parameters for the impeller are listed below.

- Specific speed: 1.42
- Inlet flow coefficient: 0.165
- Head coefficient: 0.400
- Inlet Mach number: 0.326
- Total pressure ratio: 1.109

Note: The difference in specific speed, head coefficient, and total pressure ratio is due to the difference in total pressure between impeller outlet and stage outlet.

Typical impeller shapes as a function of inlet flow coefficient are presented in Figure 2.

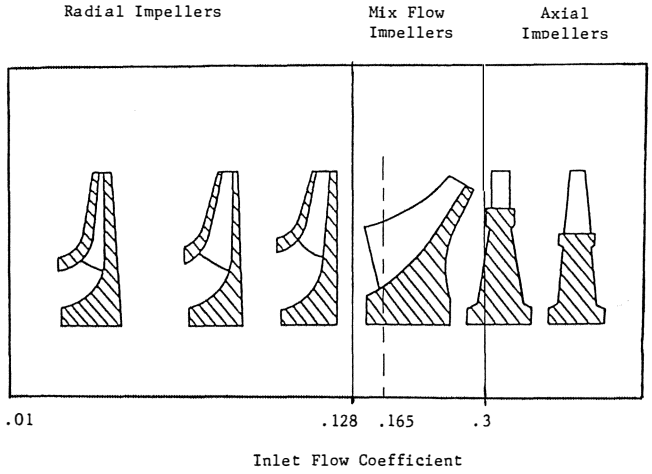

Figure 2. Typical Impeller Shapes as a Function of Inlet Flow Coefficient.

DESCRIPTION OF TEST HARDWARE

Performance testing consists of an ASME PTC 10 [2] open air performance test. The compressor is tested as an exhauster with a flow nozzle and throttle valve on the inlet. Discharge is subject to barometric pressure. The test hardware arrangement is presented in Figure 3. The description of the basic configuration is as follows. The inlet to the compressor consists of two lengths of pipe open to barometric pressure. The first length of pipe is the flow measuring section or nozzle run. The nozzle run is a 30 in diameter pipe, five pipe diameters in length, thus satisfying PTC 10 [2] criteria. The lo-beta ASME flow nozzle measures 17.973 in. Just ahead of the nozzle run are four nozzle temperature measuring stations equally spaced in a radial pattern. Nozzle static pressure references barometric pressure. Nozzle throat pressure is measured via two taps spaced 90 degrees apart and located one-half pipe diameter downstream of the nozzle inlet. The nozzle run configuration is presented in Figure 4. The remaining inlet piping downstream of the nozzle run is assembled to give accurate inlet conditions in accordance with PTC 10 [2]. The overall pipe length is equivalent to 10 pipe diameters. Four inlet static pressure taps spaced at 90 degree intervals are located four diameters upstream of the compressor suction. Four inlet temperature stations using type "J" thermocouples are located two and one-half pipe diameters upstream of the compressor suction. Discharge temperatures are measured at four measuring stations spaced 90 degrees apart and located directly at the compressor discharge flange. Pressure measurements are collected via the scanivalve system. Stations are defined to ensure that the data received are statistically significant. Fluctuations outside the limits of PTC 10 [2] (Table 2 within PTC-10) are cause for rejection.

As it was desired to measure impeller performance along with overall stage performance, modifications were made to the compressor hardware to incorporate additional test instrumentation. The challenge was to locate the instrumentation at the closest

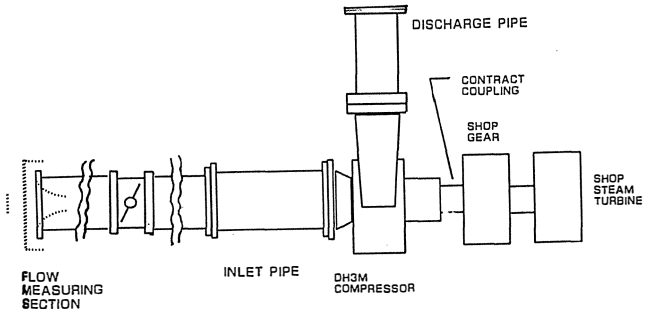

Figure 3. Test Setup to Measure Flange to Flange Performance.

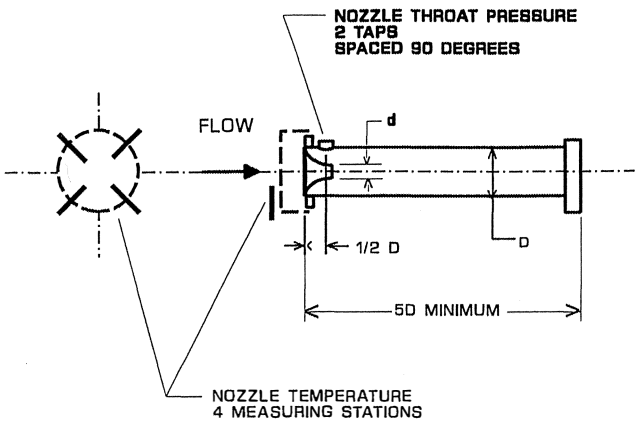

Figure 4. Nozzle Run Configuration.

proximity to the impeller. The proximity was important due to the expectation of unwanted heat transfer from the surrounding stationary aerodynamic elements. Total pressure, static pressure, and total temperature taps, four each, were incorporated as close as practical to the suction and discharge of the impeller. The static pressure was measured by drilling four holes at the inlet and discharge of the impeller. Kiel probes were used to obtain total pressure measurements at the impeller outlet. Kiel probes have the desirable characteristic of being able to take considerable deviation in the flow angle without sacrificing a great deal of accuracy. The probes are aligned to the flow based upon the predicted flow angle. Four static pressure taps are located at the inlet of the impeller near the shroud. Four static pressure taps are located at 110 percent of the outside diameter of the impeller. Four total temperature probes are located at 110 percent of the outside diameter of the impeller. Four total pressure taps are located at 110 percent of the outside diameter of the impeller. Two total temperature taps are located just upstream of the IGV. A description of the impeller measurement hardware is presented in Figure 5.

DATA ACQUISITION AND CONTROL SYSTEM

The data acquisition and control system hardware consists of a custom configured intelligent acquisition/control unit (DAC) in communication with two computers. The DAC, in turn, is connected to and controls other instruments, including a device for measuring vibration and a scanivalve system for measuring pressures less than 500 psia. Once programmed by downloading from the controlling computer, the system continuously scans and reads all of the above signals and directly stores them in engineering units, independently from the computer. All calibrations are also done independently from the computer. The DAC data are written to their own hard drive every one and one-half minutes and are kept as a semipermanent record that can be reviewed for trends or other relevant information. The second computer serves as a data monitor during tests. It is preformatted

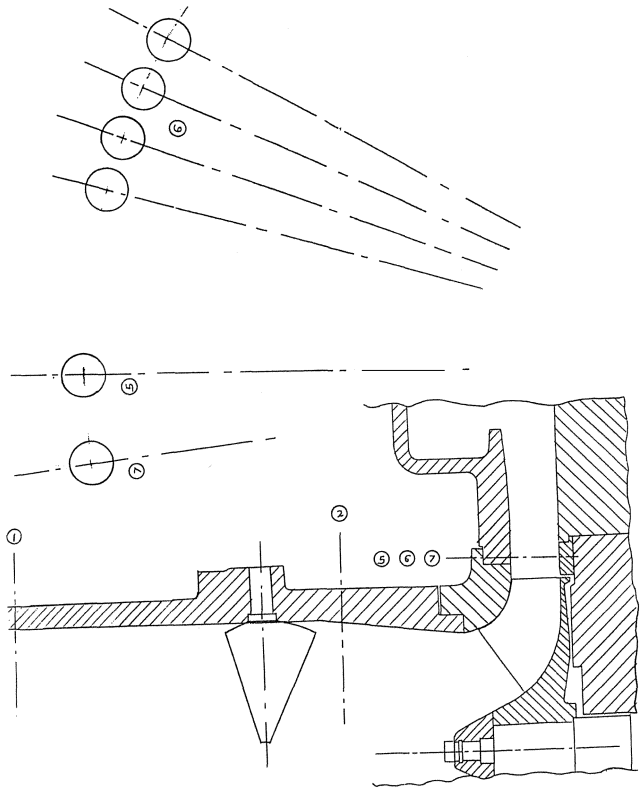

Figure 5. Test Setup for the Measurement of the Impeller Data.

before the test and displays data at specified intervals in labeled data sheet form. Up to 260 items (20 data sheets) can be displayed for one test. Two tests can be monitored concurrently. The main computer controller is used for general system supervision, mechanical data analysis, and conducting the analysis of performance testing.

The overall performance test was conducted in accordance with ASME PTC 10 [2]. Additional data were taken for a zero degree inlet guide vane setting over the full range of the performance curve. This test was duplicated at the zero setting over the full range of the curve. The inlet guide vanes were repositioned to obtain data across the full range of the curve for additional settings. These data are used to determine the influence of counter swirl (−IGV settings) and preswirl (+ IGV settings) on the performance of the impeller. The description of the IGV configurations tested is presented in Table 1.

Table 1. Tested Inlet Guide Vane Configurations.

0° IGV - Full Curve
Repeat 0° - Full Curve
−10° - IGV Full Curve
−20° - IGV Full Curve
+15° - IGV Full Curve
+30° - IGV Full Curve
+45° - IGV Full Curve
+60° - IGV Full Curve
+80° - IGV Full Curve

DESCRIPTION OF TEST PROCEDURES

The test gas for all points is air. Test calculations are performed as per PTC 10 [2] Class III methods. Test gas properties are determined from stored lookup tables based on a mixture of dry air

and water vapor consistent with the measured wet- and dry-bulb temperatures. The test speed, which is 10 percent higher than the design speed, is matched to actual conditions at the time of the test to provide a test volume ratio within five percent of the actual test results corrected to specified conditions. No Reynolds number corrections are applied to results. Pressures are measured with a scanivalve and a zero to 50 psia transducer. Transducer 'zero' is calibrated automatically during each data scan against barometric pressure. Nozzle differential pressures are calculated from individually measured nozzle and throat static pressures. Estimated flow nozzle error tolerance is ± 0.5 percent. The overall stage efficiency and corrected shaft power are calculated based upon enthalpy rise measurements across the compressor. Casing and ambient temperatures are measured as a part of the data.

The impeller was run at 10 percent higher than design speed to increase the temperature rise across the stage. The elevated temperature of the lubricating oil in the bearing housing, impeller, and shaft is known to migrate into the casing, raising the temperature of the casing and eventually the scroll. This has a negative effect on calculated efficiency as the temperature rise across the impeller can be artificially influenced by this heat migration. The low temperate rise across the stage in consideration makes it even more susceptible to error. In this case, even 1°F inaccuracy could result in a five to six point error in impeller efficiency calculations. The effect of 1°F error in temperature measurements to percent error in impeller polytropic efficiency is presented in Table 2.

Property of Gas:

Gas = air, K = cp/cv = 1.4, Z = 1.0, MW = 28.79

Table 2. Effect of 1°F Error on Impeller Polytropic Efficiency.

Sr No	Inlet Total Temp T1 °F	Discharge Total Temp T2 °F	Incorrect Discharge Total Temp °F	Inlet Total Pressure P1 psia	Discharge Total Pressure P2 psia	Imp Poly Eff ETA p	Incorrect Imp Poly. Eff. ETA pinc	% Error ETA p-ETA pinc
1	79.14	96.59	97.59	13.182	14.482	0.840	0.800	4.4%
2	82.55	98.13	99.13	13.326	14.465	0.830	0.779	4.9%
3	82.70	96.30	97.30	13.551	14.518	0.800	0.741	5.4%
4	79.05	94.42	95.42	13.183	14.427	0.920	0.861	5.5%

Measured test data for the design condition are presented in Table 3.

Table 3. Measured Test Data—Design Conditions.

Reading No	Static Pressure in PSIA after IGV Location 2				Static Pressure in PSIA at Inlet of Diffuser (1.1*D2) Location 5			
Design point	P11	P12	P13	P14	P15	P16	P17	P18
1	13.072	13.066	13.054	13.06	14.065	14.09	14.137	14.122

Total Pressure in PSIA at Inlet of Diffuser (1.1*D2) Location 6				Total Temp in °R at Location 1	
P19	P20	P21	P22	T11 °R	T12 °R
14.328	14.546	14.557	14.610	538.73	538.70

The results of test data calculations for the design condition are presented in Table 4.

Table 4. Results of Test Data Calculations.

Reading No	Avg St Pressure at Loc 2 psia	Avg Tot Pressure at Loc 2 psia	Avg Tot Temp. at Loc 1 °R	Avg St Pressure Loc 5 psia	Avg Tot Pressure Lot 6 psia
1	13.063	13.183	538.715	14.104	14.510

The results of test data calculations from ASME PTC 10 [2] test code are presented in Table 5.

Table 5. Results of Test Data Calculations Per PTC-10 [2] Code.

Inlet Flow Ft3/min at Loc. 2	Mass Flow lb/min	Impeller Speed rpm	K	Z	MW
27650	1815	3275	1.4	1.0	28.79

DISCUSSION ON APPLICATION OF CFD CODE IN CENTRIFUGAL COMPRESSOR DESIGN

CFD fluid flow analysis is a relatively new field that has gained increased acceptance in centrifugal compressor applications in recent years. This tool gives engineers increased understanding of the fluid flow behavior within specific components. If applied successfully, it has the potential of reducing the number of iterations and costly experimental test trials. The overall design cycle for new applications may be greatly reduced. However, the results obtained from the CFD code can only be considered qualitative rather than quantitative unless verified by actual experimentation. Potential for uncertainty in the CFD code results could arise when one tries to model turbulence. Various codes use different turbulence models. As most of the turbomachinery has some turbulent flow, the accuracy of the results depends upon how effectively the CFD code models turbulent flow. If the given turbulence model does not represent turbulent flow correctly, significant error could occur, especially in the boundary layer region near the walls (suction and pressure side of the blade, hub and shroud portions coming in contact with the fluid). The analysis code, in this case, uses a well known K-epsilon turbulence model. Generally, the CFD code is best applied to give a relative comparison of successive trials for a given impeller. The absolute values are considered to be approximate, unless it is corroborated by the experiment. Thus, if the turbulence model is calibrated against actual test data, it can give reliable results.

In the present analysis, the measured total and static pressures at given locations were compared with the CFD calculations and both were found to be in excellent agreement.

A comparison between measured test data and the calculations from the CFD calculations for design condition at measurement locations is presented in Table 6.

Table 6. Test Data vs CFD Code Calculations.

Name	Units	Location	Measurements from Test	Calculations by CFD Code	% Error
Avg. st. press.	psia	2	13.063	13.065	0.015
Calc. avg. total press.	psia	2	13.183	13.184	0.007
Avg. st. press.	psia	5	14.104	14.142	0.26
Avg. tot. press.	psia	6	14.510	14.550	0.28
Avg. tot. temp.	°R	2	538.715	539.126	0.076

The results of the impeller performance calculations from CFD code for the design condition are presented in Table 7.

Table 7. Calculation of the Impeller Performance by CFD Code.

Total Press at Imp Inlet PO_{1imp} psia	Total Press at Imp Outlet PO_{2imp} psia	Total Temp at Imp Inlet TO_{1imp} °R	Total Temp at Imp Outlet TO_{2imp} °R	Imp Efficiency
13.178	14.611	539.328	556.824	0.924

K = cp/cv	Z	MW	R = 1545.4/MW	Imp poly head ft
1.4	1.0	28.79	53.6784	3037

Thus, one can conclude that the quantitative values calculated by the CFD code will help the user in calculating the performance of the given impeller.

DESCRIPTION OF CFD MODEL AND CFD CODE

The computational fluid dynamics analysis code used by the authors was developed by a computing company in Canada. It incorporates a preprocessor and a flow solver. The flow solver provides solutions for incompressible or compressible, steady state or transient, laminar or turbulent fluid flow in complex rotating and nonrotating geometries. The preprocessor uses block structured nonorthogonal grids with grid embedding and grid attaching to discretize the domain. When using the preprocessor, it is necessary to specify the thermodynamic and transport properties of the fluid. The preprocessor uses time dependent Reynolds stress averaged Navier-Stokes equations. It also employs the K-epsilon turbulence model [3] to account for the turbulence fluctuations from mean. The intent here is not to provide full theoretical background and all governing equations used in the analysis code, but to concentrate on the application of the code in the field of turbomachinery.

The program resides on a computer workstation. A fine grid for one impeller flow passage, with the blade in the center of the passage, was generated using the software's preprocessor. The resulting model consists of 104,544 nodes. The impeller model is presented in Figure 6. The inlet and discharge extensions were constructed such that they closely resemble the inlet and the discharge flow passages. The given domain is broken up into discrete subdomains. The grids acceptable to the flow solver are boundary fitted, generally nonorthogonal, and curvilinear. Boundary conditions were applied and test conditions consisting of the total temperature and the total pressure at the inlet, the mass flow at the discharge, and the impeller rotational speed were input. The total solution time was approximately 12 hours. The results were analyzed using the postprocesser. The accuracy of the results is dependent upon the agreement with the code prediction compared against measured results for the static pressure and the total pressure. Agreement of these parameters would allow a correlation to be drawn between actual performance and code predictions of the impeller aerodynamic efficiency.

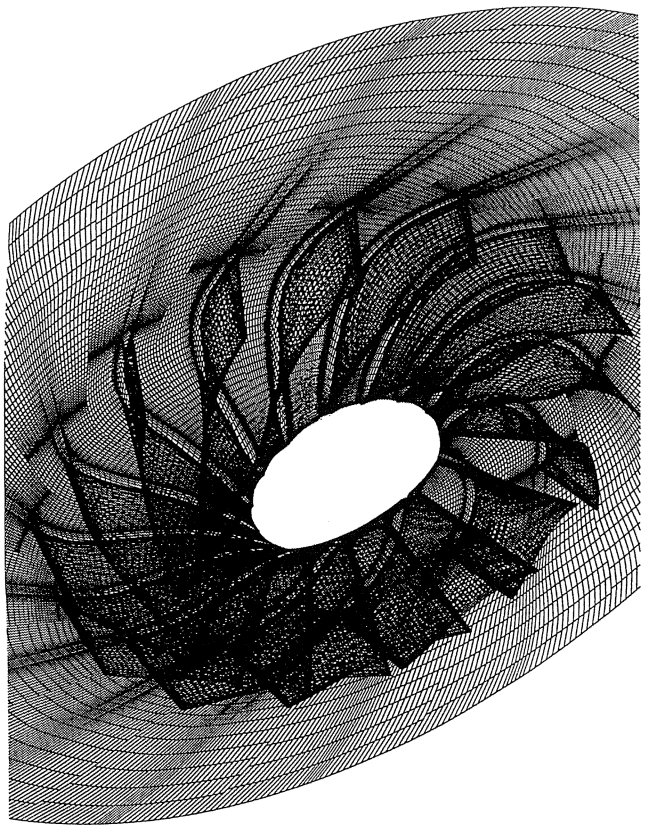

Figure 6. Impeller Model by CFD Code.

Input Information to the CFD Code

The CFD code requires substantial user input information. This information is distributed in several different files that are used by the flow solver. The geometry of the impeller is stored in a data subdirectory. In the process of generating a grid, the code proceeds through a geometry phase, curve phase, surface phase, and grid generation phase. Each phase is handled by subprograms of the preprocessor. The grid size, grid density, node distribution, boundary conditions, maximum number of iterations, convergence criteria, and gas properties are specified in various files.

Since the impeller has identical passages equal to the number of blades, it is not necessary to model the whole impeller. Only one passage is modelled with the blade in the center of the passage and half of the passage on each side of the blade. This reduces the number of nodes, the memory requirement of the hardware, and the calculation time considerably. It is assumed that all the other passages are identical to the selected passage and have the same boundary conditions. The geometry of the blade is simplified by using straight line elements for which the coordinates of the endpoints of each straight line are required. The straight line elements of the given impeller are presented in Figure 7.

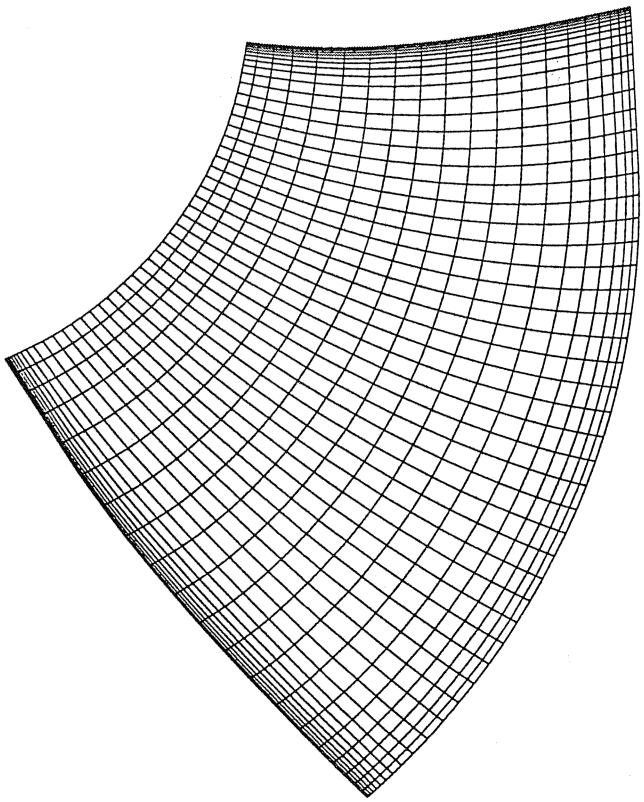

Figure 7. View of the Impeller's Blade with Straight Line Elements.

For CFD calculations, the upstream and the downstream geometry must be included. It is desirable to have them match as closely as possible to the actual inlet and outlet geometry of a given impeller. The boundary conditions should be applied at the location where actual measurements are taken. The cross sectional view of the given passage, including inlet and exit extensions, and the station (location) numbers are presented in Figure 8.

Output Results from the CFD Analysis

Once the converged solution from the CFD code solver is obtained, a substantial quantity of information is generated that is stored in various files. A diagnostic report of the flow solution is

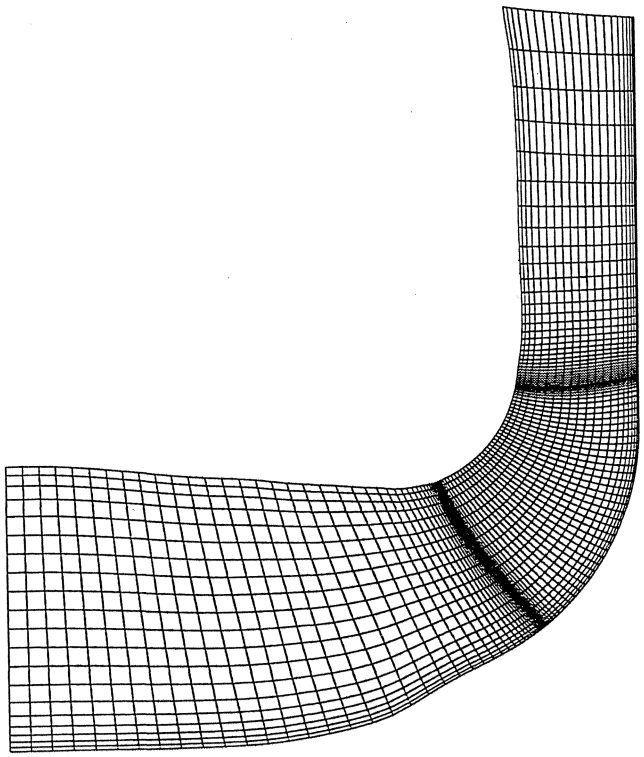

Figure 8. Cross Sectional View of Impeller Passage with Inlet and Discharge Extensions.

found in .OUT file. In the .OUT file, one can see the history of the total run, including the number of iterations, mass, momentum, and energy balance summary, convergence criteria, and a summary of each iteration. Following verification of the .OUT file and if all the necessary criteria for convergence are met, the next step is to plot and calculate various fluid flow parameters and evaluate the performance of the given impeller. The plots are useful in visualizing the flow in the impeller passage and can be used to identify where the maximum losses occur. This information can be used to make further improvements in the analyzed geometry. Some of the useful plots are the velocity vector plots, the relative total pressure plots, and the relative velocity plots. The velocity vector plot in the I plane (meridional direction) at midpassage is presented in Figure 9. The vectors indicate the magnitude and the direction of the velocity. Any low velocity vector fields and any reverse flow fields can be identified from this output. The relative total pressure fringe plot in the I plane (meridional direction) at midpassage is presented in Figure 10. In ideal fluid flow (no losses), the total relative pressure remains constant. But in real fluid flow various losses occur, and wherever the relative pressure is low the losses are high. This plot aids in identifying high loss regions. It is necessary to look at the above mentioned plots at various I planes along with J and K planes. The details about the I, J, K planes are presented in Figure 11.

CONCLUSION

A CFD model was generated to duplicate the geometry of an impeller under investigation. Stations for performance prediction were established within the model. The results obtained from the CFD calculations were compared with measurement data taken at the same locations in the tested compressor. Excellent agreement between measured and calculated pressures was obtained. This provided a great degree of confidence in the ability to accurately calculate the performance of the impeller. The CFD analysis also gave improved understanding of the flow and loss distribution in the impeller. This information proves valuable in that it allows for

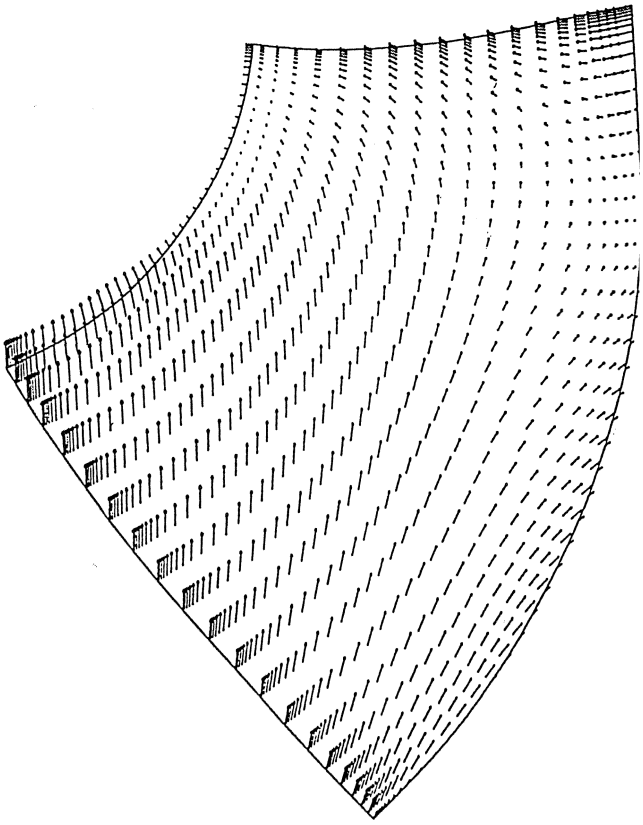

Figure 9. Velocity Vector Plot at Blade Midpassage.

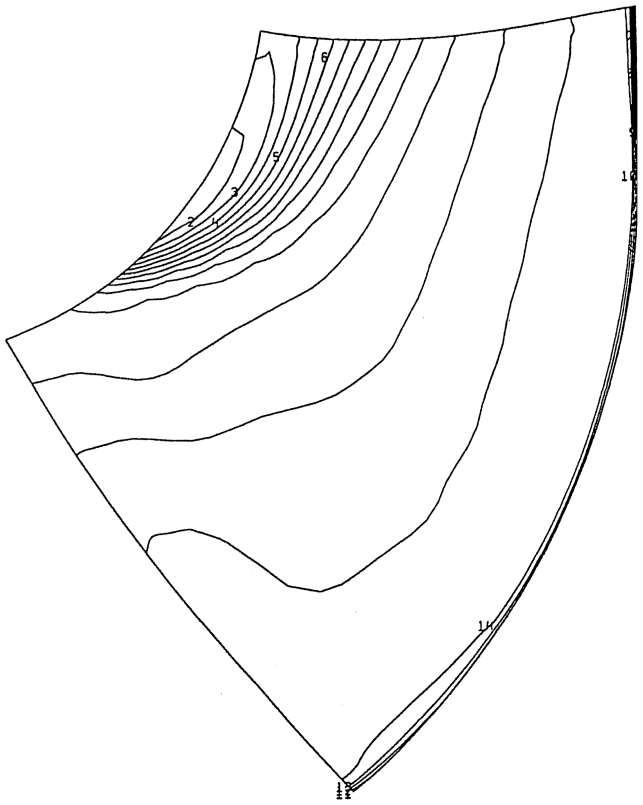

Figure 10. Fringe Plot of Relative Total Pressure at Blade Midpassage.

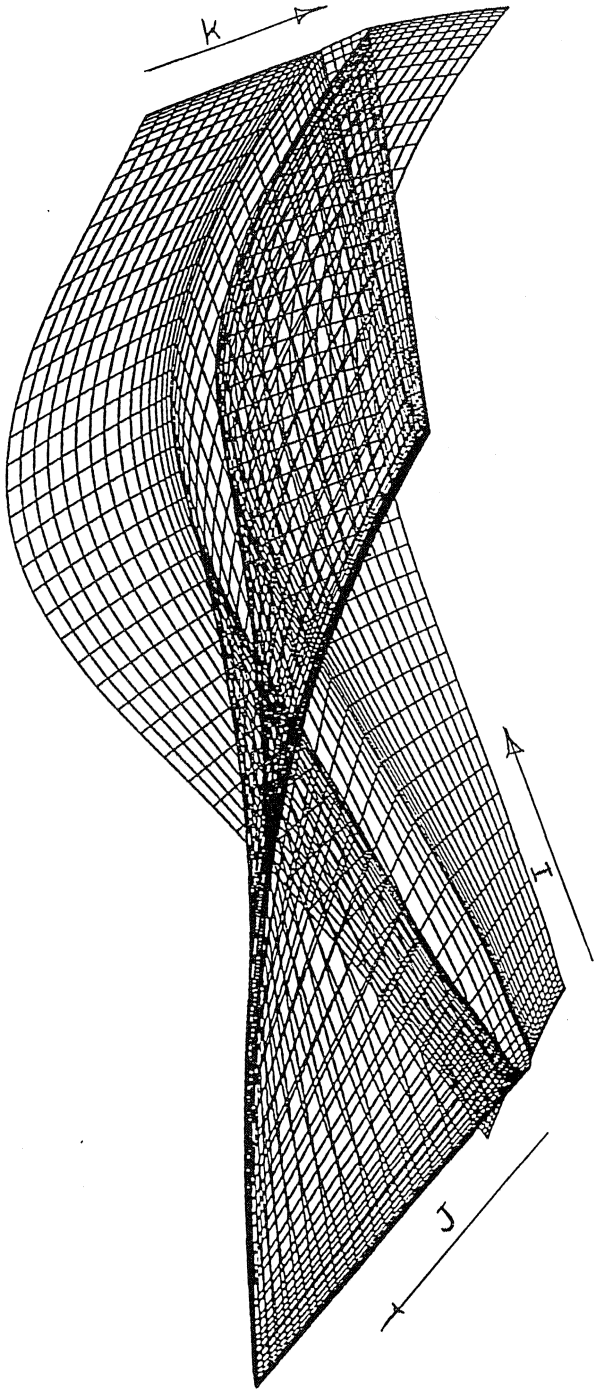

Figure 11. Details of I, J, and K Planes.

future enhancement of the design. Additionally, the designer is able to better calibrate the coefficients used in one dimensional calculations. The conclusions drawn from the combination of CFD analysis and limited test data would not have been possible without an alternate (and substantially costlier) test configuration.

APPENDIX

Sample Calculations:

Calculations for Table 4.

1. Average static pressure at location 2

$$P_{@2static} = \frac{P_{11} + P_{12} + P_{13} + P_{14}}{4} = 13.063 \text{ psia}$$

2. Average velocity at location 2

$$V_{@2} = \frac{Q_{inlet}}{A_{inlet}} = 130.367 \text{ ft/sec}$$

3. Average total pressure at location 2

$$P_{@2\ total} = P_{@2\ static} + 1/2\ \rho\ V_{@2}^{\ 2} = 13.183 \text{ psia}$$

4. Average static pressure at location 5

$$P_{@5\ static} = \frac{P_{15} + P_{16} + P_{17} + P_{18}}{4} = 14.104 \text{ psia}$$

5. Average total pressure at location 6

$$P_{@6\ total} = \frac{P_{19} + P_{20} + P_{21} + P_{22}}{4} = 14.510 \text{ psia}$$

6. Average total temperature at location 1

$$T_{@1\ total} = \frac{T_{11} + T_{12}}{2} = 538{,}715^{\circ}\text{R}$$

Calculations for Table 5 are based upon ASME-PTC 10 [2] code.

Calculations for Table 7:

1. Impeller Polytropic efficiency

$$\eta_{p)imp} = \frac{\left(\frac{k-1}{k}\right)\left(\ln\left(\frac{(PO)_{2imp}}{(PO)_{1imp}}\right)\right)}{\ln\left(\frac{(TO)_{2imp}}{(TO)_{1imp}}\right)} = 0.924$$

2. Impeller Polytropic head

$$H_{p)imp} = \frac{zRk\eta_{p)imp}(TO)1\ imp}{(k-1)}\left[\left(\frac{(PO)_{2imp}}{(PO)_{1imp}}\right)^{\frac{(k-1)}{(k)(\eta_{p)imp}}} - 1\right] = 3037 \text{ ft}$$

REFERENCES

1. "TASCflow User Documentation," Advanced Scientific Computing Ltd. (October 1992).
2. ASME PTC 10, Compressors and Exhausters Power Test Codes.
3. Launder, B. E. and Spalding, D. B., "The Numerical Computation of Turbulent Flows," Comp. Meth. Appl. Mech. Eng., *3*, pp. 269-289 (1974).

BIBLIOGRAPHY

TASCgrid chapter of the "TASCflow User Documentation," Advanced Scientific Computing Ltd. (October 1992).

ACKNOWLEDGEMENTS

The authors would like to acknowledge the significant contributions offered by Russel W. John. Since his retirement from A-C Compressor, Mr. John has served in a consulting role. Recognition is due to Andrew Gerber of American Scientific Computing. The authors would also like to thank Henry Parker, Patrick Shay, and Mary Anne Strite from the testing department. The authors also acknowledge Thomas Feller, Joseph Cruickshank, and others in the preparation of this paper.